Single-grain dose-distribution measurements by optically stimulated luminescence using an integrated EMCCD-based system

Greilich, S.[a,*], Gribenski, N.[b], Mittelstraß, D.[c,d], Dornich, K.[c], Huot, S.[e], Preusser, F.[b,f]

[a]*Department of Medical Physics in Radiation Oncology, German Cancer Research Center (DKFZ), Im Neuenheimer Feld 280, D-69120 Heidelberg, Germany*
[b]*Department of Physical Geography and Quaternary Geology, Stockholm University, 10691 Stockholm, Sweden*
[c]*Freiberg Instruments, Delfter Straße 6, 09599 Freiberg, Germany*
[d]*Department of Geography, Justus-Liebig-University, Senckenbergstr. 1, 35390 Gieen, Germany*
[e]*Département des sciences de la Terre et de l'atmosphère, Université du Québec à Montréal, CP 8888 Succ. Centre-Ville, Montréal, Québec, Canada H3C 3P8*
[f]*Present address: Institute of Earth and Environmental Sciences - Geology, University of Freiburg, Albert Straße 23-B, 79104 Freiburg, Germany*

Abstract

We report on the feasibility of assessing single-grain dose-distributions by using an EMCCD-based imaging system with complementary analysis software. Automated image-processing was successfully applied to compensate sample motion and for automated grain identification. Following a dose recovery test, 74 % of the grains were recognized successfully, and 44 % exhibited a suitable OSL dose response behavior to interpolate an equivalent dose value and a central dose recovery ratio of 1.038 was obtained.

Keywords: spatially resolved luminescence, OSL, TL, luminescence dating, Lexsyg reader

1. Introduction

Luminescence dating is based on the measurement of a signal emitted by minerals such as quartz and feldspar during light stimulation. Traditionally, this signal is detected by a photomultiplier tube (PMT), collecting without distinction photons expelled by several hundreds to thousands grains at the same time. Individual grains of a sample can, however, differ in terms of their initial and overall luminescence emission output and behavior. This

*Corresponding author, Tel: +49-(0)6221-42-2632, Fax: +49-(0)6221-42-2665
Email address: s.greilich@dkfz.de (Greilich, S.)

can be due to variation in radiation sensitivity and saturation characteristics but also partial bleaching, multiple events or post-deposition disturbance recorded in the sample. When analyzing a signal integrated from several grains , this essential information is lost and wrong age estimates can result [1]. The determination of equivalent dose distribution on a single grain level can, in contrast, reveal the presence of partial bleaching or mixed grain populations [21], allowing to extract sub-population of interest by using statistical tools such as the Minimum Age Model [11] or the Finite Mixture Model [10]. The first attempts of single grain equivalent dose measurements using OSL were carried out by Lamothe et al. [17] and Murray and Roberts [19], who hand-picked each grains on individual aliquots and measured them one by one; a laborious and time consuming procedure. The approaches that have been pursued subsequently can be grouped into two principal strategies: Either the entire sample is stimulated simultaneously and a detector records the spatial luminescence intensity distribution (imaging) or confined parts of the sample are stimulated subsequently and any suitable photon counting device can be used for OSL detection (scanning). Both methods have to provide the accurate assignment of OSL intensity to a specific grain, which uncertainties in the definition of the area of signal integration, signal cross talk between adjacent grains, and variability in mechanical position of the sample during repeated irradiation and readout militate against.

The most widespread single grain system, an automated Risø reader with additional laser-scanning head [8], uses sample holders with 100 holes to host sunk-in single grains and a system of landmarks. This allows for assignment of the OSL intensity to individual grains. However, laser position, power fluctuation and non-uniform irradiation can yield variation in recorded luminescence which is not due to the respective grain properties [2]. Also, grains have to be removed from the original context, which for example deteriorates potential information on small-scale dose-rate variation [26].

More recently and with the advent of affordable, highly sensitive charged coupled devices (CCDs) and electron multiplier CCD (EMCCDs) it was shown that luminescence dating of stone surfaces [13, 12] and sediment samples [22, 4] based on the imaging approach is within

reach. This would allow the simultaneous stimulation of all grains in a sample, avoiding problems of laser scanning, and thus a wide choice of light sources and potential samples (grain size, sample preserved in their original context etc.).

To constitute a viable alternative in luminescence dating with a sufficiently large number of grains, a process for automated identification (segmentation) of random grains and compensation of misalignment (registration) has to be accessible which is not yet the case. In this article, we therefore report on the feasibility of routine single grain OSL dating by using a novel, EMCCD-based, integrated system with appropriate image-processing. We believe that three major issues have to be solved to implement the method: sample motion, automated grain identification and signal cross-talk, where we investigate the first two while the latter will be subject of a separate study.

2. Equipment

2.1. Luminescence Reader

All measurements were performed with a Freiberg Instruments Lexsyg research luminescence reader (Fig. 1), built in 2012 and nicknamed Delorean. In addition to a UV-Vis- and a Vis-NIR-photomultiplier tube mounted besides the used EMCCD camera on a detector changer, the device is equipped with a solar simulator consisting of a multi-wavelength power-LED-array [24] used for bleaching the sample before experiments. For dose regeneration with β-radiation a $^{90}Sr/^{90}Y$ ring source was used. It delivers a dose rate of about $0.0511\,Gy{\cdot}s^{-1}$, with a variation of less than $5\,\%$ over the aliquot area [23].

2.2. Detector

To perform spatially resolved measurements, Delorean is equipped with a Princeton Instruments ProEM512B eXcelon EMCCD camera (ex works, [24]). The camera features a backilluminated, UV-fluorescence-coated e2v CCD97 sensor ($512{\times}512$ pixels, 16x16 μm^2) which generates images of 16-bit signal depth. The sensor arrays quantum efficiency is approximately $45\,\%$ (380 nm UV quartz emission), $70\,\%$ (410 nm feldspars emission), or 85-$95\,\%$ (visible range), respectively [16]. The device was operated in Electron Multiplier (EM)

mode. In this mode, the photoelectrons induced by incoming photons are multiplicated before electron-to-count conversion by a high voltage gain register. This increases the signal level in proportion to the read out noise and therefore enhance the signal-to-noise ration in low light applications [28].

2.3. Optics

The optical setup comprises a lens for light collection built into the OSL stimulation unit and independent of the detector chosen. Two additional lenses attached directly to the camera, focus the image onto the CCD. All lenses are spherical, made of fused silica and have UV/Vis antireflection coating. The setup was calculated to have a numerical aperture (NA) of 0.526, a transmission of $\approx$97 % (at 365$\pm$25 nm), and a magnification of 0.89 (mapping value 18 µm per pixel). The high NA spherical lenses cause considerable spherical aberration. The experimental obtained Michelson fringe visibility (image contrast) of an interference pattern (2 line-pairs / mm, corresponding to a 250 µm structure) is about 30 % in the inner 4 mm image area and decreases further towards the field-of-view edges due to the secondary effect of astigmatism. Practically, this leads to blurry images and halos around a luminescent grain (Fig. 4). On the other hand the setup has the advantage of increase depth of field, minimizing the effects of chromatic aberrations or sample height variation and thus dispensing the need for refocusing with respect to the detection wavelength or sample.

2.4. Sample discs and reflective images

Preliminary tests showed the necessity of obtaining reflective light images (photos) after each record. On the one hand, they are used to correct the positioning uncertainty of the sample arm (see 3.1.2). Also they serve as reference pictures for the grain detection algorithm (see 3.2). Therefore, special stainless steel sample discs of 10 mm diameter with mirroring surface were developed. They had been polished to remove potential stray light by reflecting the angular irradiating stimulation light to the opposite direction and not towards the camera optics.

2.5. Stimulation light and detection filters

For the experiments, blue stimulation light with an intensity of 60 mW/cm^2 at the sample was used, achieved by a ring five power LEDs narrowed to 458±5 nm by filters [24]. For OSL, the detection window was set from 340 nm to 390 nm (2.5 mm Hoya U340 and a Delta BP 365/50 EX interference filter). For reflected light images, no color filters were employed but overexposure was prevented by a ND40B neutral density filter (ThorLabs, optical density 4.0) and an additional aperture with 8.5 mm inner diameter limited spherical aberration and reflection caused by stimulation light flares.

2.6. Measurement software

The sequences were built using LexStudio2 version 1.0.6c (January 2014) with the new developed "photo" sequence command to take reflective images after each OSL measurement. The blue LED stimulation (458±5 nm) was used as flash light. The image acquisition was performed with Princeton Instruments WinView version 2.6.18 (September 2013). Image exposure was triggered automatically by LexStudio2 using the cameras external synchronization port. For data evaluation, AgesGalore2GUI version 0.1.0.3 (March 2014) was applied, using ImageJ version 1.48r (developers build, February 2014) and AgesGalore2 build 746 (February 2014) as function libraries.

3. Image and data processing

The methodical work flow of single grain dose evaluation using an EMCCD detector can be divided into three main steps: (i) image stack correction, (ii) region-of-interest definition per grain, (iii) single grain equivalent dose calculation (Fig. 2).

To achieve the first and the second step, image processing methods were evaluated. The Public Domain biomedical image processing software ImageJ [27] was used as function library and plug-in platform. The third step, the equivalent dose evaluation, is performed by the free commando line based luminescence dose calculation software AgesGalore2, a lean redefined successor of AgesGalore [12]. Both software utilities are embedded in the

free graphical interface software AgesGalore2GUI[18][1].

AgesGalore2GUI serves as input mask for all major algorithm parameters, displays the analysis results and performs the data file and sub-program handling[2]. It reads the Freiberg Instruments LexStudio2 sequence record (XSYG file) to register the images. Although it is optimized for Freiberg Instruments lexsyg data, when processing the image registration manually and eventually pre-formatting the image stack file, AgesGalore2GUI can be used to evaluate none-lexsyg CCD luminescence measurements too. For this study the AgesGalore2GUI alpha version 0.1.0.3 (March 2014) was used.

3.1. Image manipulation

Preliminary tests have shown, that raw image data are corrupted by the following effects:

- Randomly falsified CCD areas by the impact of high energy photons
- Translated grain locations by not reproducible aliquot positioning deviation
- Signal cross talk of nearby grains by optical aberrations (blurring)

The first two issues were solved by applying image processing methods, realized in an AgesGalore2GUI controlled ImageJ macro. The last issue will be investigated in a separate study.

3.1.1. Cosmic ray and secondary X-ray impact removal

The ImageJ provided Outlier removal algorithm can decrease the influence of impacts of secondary x-rays (*bremsstrahlung*) due to the nearby beta source and cosmic rays on the

[1]Both distributed freely under GNU General Public License v3. They can be used, redistributed and modified freely. The copyrights lay by Steffen Greilich (AgesGalore2) respectively Freiberg Instruments GmbH (AgesGalore2GUI). The copyrights and terms of use of ImageJ and his Plug-ins remain by their owners.

[2]The GUI is programmed in C# using the .NET Framework 4.5 Process Class functionality to control a Java Virtual Machine where ImageJ and AgesGalore2 are executed by commando line scripting.

CCD [9]. Those rays cause small areas of a few pixels to have values up three to four orders of magnitude above the OSL signal. If an impact occurs inside a region-of-interest, the related L_x/T_x value would be falsified, distorting the dose response curve of the grain. The algorithm identifies the corrupted pixels by comparing them to the median of the surrounding pixels and replaces them with this median value if they are above a user-set threshold.

3.1.2. Image alignment

Over repeated measurements, the positioning uncertainty of the sample arm, though less than 50 µm, combined with sliding and rotating due to the arm velocity, can lead to a displacement of the sample carrier relatively to the detector of up to around 180 µm. Therefore, if the the grains location on the CCD picture moves, grain definition and dose response curve calculation would be corrupted. The TurboReg registration plug-in [29] identifies both translational and rotational sample displacements between two images. In AG2-GUI, this plugin uses the light reflected pictures, which have been taken after each measurement steps. An ImageJ macro sets the first reflective image of the observed image stack as the reference and sets later reflective images as targets. The TurboReg plug-in minimizes the mean-square difference between reference and target and calculate the rotation and translation parameters from some automatically set landmarks. The macro then applies these parameters not just at the target but also on luminescence images progressed before the targeted reflective images was taken, assuming that no sample arm movement happened between them. In this way, the whole image stack is aligned. To prevent edge effects corrupting the grain definition algorithms, a circular mask is drawn after applying the plug-in[3].

[3] The size of this mask is calculated from the maximum detected aliquot movement, and pixels of the outer region of the mask are set to the mean pixel value of the inner region, overwriting all invalid image regions.

3.2. Region of Interest definition per grain

3.2.1. Image segmentation strategy: Grain boundaries as ROI

With the current system, using a Lexsyg reader and an EMCCD camera, digital images records the spatial distribution of luminescence emitted by grains spread over a flat aliquot surface. To attribute a signal per grains, it is therefore necessary to segment the image in regions of interest (ROIs) which will select clusters of pixels per grains. Two approaches can be applied for segmenting the images. Firstly, focusing on luminescent spot areas and segmenting directly on luminescence images (*a posteriori* segmentation). To isolate areas of bright signal spot emitted by individual grain, a background has to be removed. However, due to the necessity of brightness gradient between the grains, only the brightest grain will be considered while other grains, although bright enough for OSL traditional analysis (SAR, etc.), will be disregarded. In addition, such segmenting approach can yield large ROIs per grain, which are in turn more susceptible to integrate signal emitted by surrounding grains. The second alternative is to define fixed geometrical areas for every grain and to analyze each signal integrated across these areas (*a priori* segmentation). By doing so, one does not aim to include all the pixels exhibiting a luminescence signal, but only those that were found beforehand to belong to a specific grain. Here, we assume that the signal recorded from the area corresponding to the physical grain is not contaminated by signal emitted by surrounding grains (cross talk), as long as a sufficient distance is kept between the grains (Fig. 3). As this effect is not clearly visible on the luminescent pictures, the identification of the grain boundaries (and whole segmentation procedure) is done using the light reflected pictures of the aliquot.

3.2.2. ROI segmentation workflow

Firstly, to automatically identify the grains boundaries, these objects have to be clearly distinguishable from the background, which is inconstant on the light reflected images (reflection light artifacts). The Background Substractor plug-in [3] can mitigate the variable background induced by aberrations and ADC offset. It uses a sliding window histogram approach and takes the most probable value as local background estimate. The side-length

of the sliding window has to correspond to (or to be slightly larger as) the diameter of the largest object, i.e. grain Then the Threshold plug-in is applied to the pixel values as a first step of grain identification. This approach will transform a grey scale image in a binary image, with one color representing the pixels of interest, and the other the pixels disregarded (background). The plugin provides a choice of numerous algorithms for threshold computing from which will highly depends the binary image resulting (Fig. 4). Once the image has been correctly segmented, the ImageJ Watershed algorithm [9]recognizes notched areas and dissects them at their narrow point, assuming the areas displayed two overlapping grains. The ImageJ Analyze Particle command converts this into ROIs. It uses geometrical constraints of the objects sought after set by the user, most prominently the circularity and the size ranges.

3.3. Single-grain equivalent-dose calculation

AgesGalore2 calculates the equivalent dose and the rejection criteria based on an adapted SAR protocol for every pixel and for two-dimensional integration areas (regions-of-interests). The later ability is used to handle every region-of-interests as one quasi-aliquot with one particular dose response curve, evaluated similar to common evaluation methods [7] including error propagation. AgesGalore2 is of similar structure and functionality as its predecessor AgesGalore [14] but had been redefined in a number of aspects:

- Based on the Java programming language, it has cross-platform compatibility. Thus, AgesGalore2 could be freed from unnecessary code, e.g. for handling image data, regions of interest, I/O, making the software and its development leaner and faster.
- AgesGalore2 was designed as a shell, to be controlled with text commands, scripts or a client/server connection. This allows a tiered structure and to separate graphical user interfaces and data management without intermingling with the functionality.
- The software was inherently designed to deal also with coarse grain data while its predecessor was mainly limited to rock slices.

A detailed description of the algorithms employed is given in Appendix A.

4. Experiments and results

In order to test our system, and especially the aliquot movement correction, grain boundaries ROI definition and data analysis throughput, we performed dose recovery measurements on quartz samples. Complexities linked to cross-talking are not investigated here and will be the object of a next study, as the sensitivity level evaluation of the system.

4.1. Samples

Quartz grains (160-250 μm, standard chemical pre-treatment) were extracted from plunge pool flood sediments from Litchfield National Park, Northern Territories, Australia (May et al., in prep.). According to prior multiple and single grain analyses, these samples exhibit a large number of grains emitting strong and fast component dominated OSL signal.

4.2. Experimental settings

Two aliquots with a total of around 250 grains were prepared. To limit signal cross talk, the grains were well separated by checking the disk under a stereo microscope and using a needle. The samples were bleached using the sunlight simulator for 15 min prior to he actual measurements and bleaching efficiency of the sunlight simulator unit (power of each LED at 50 %) was checked by PMT-based OSL readings. A laboratory dose of about 50 Gy (1000 s) was chosen for the dose recovery test to prevent any potential difficulties linked to the sensitivity issue (cf protocol tab 1) The Electron Multiplier port of the CCD camera was operated with an avalanche gain of x100, a register readout rate of 5 MHz, at full-chip resolution and an exposure time of 0.5 s per image.

4.3. Rate of success for different image processing parameter settings

Four parameters were systematically varied in order to find the most successful combination for the grain segmentation step: the sliding windows side length for the Background Substractor plug-in, the algorithm for the Threshold plug-in, the minimum particle and the minimum circularity for the Analyze Particles tool. The best results for the Background Subtractor were achieved using a sliding window length of 20 pixels (equivalent to 360 μm,

slightly larger as the average grain diameter). The default thresholding approach based on a variation of the isodata algorithm of [25] was found to yield best results (Tab. 2). It calculates the averages of pixels below or equal and above a threshold value test, then computes a new composite average from the two previous mean values, and repeats this process incrementing the threshold value until the latter is above the composite average. The most efficient identification of grain boundaries has been found using a minimum circularity ($= 4\pi \cdot \frac{\text{area}}{\text{perimeter}^2}$) of 0.1 and a minimum size of 50 pixel^2 (Fig. 5).

4.4. Dose recovery test

The luminescence intensities were integrated over the 185 ROIs obtained from the best setting above, using the first image (, i.e. the first 0.5 s) for the initial OSL signal and the last three images (last 1.5 s) for the background average. The equivalent dose values were calculated based on an exponential curve fitting and a Monte Carlo approach for error calculation. The minimum signal per grain to qualify for equivalent dose evaluation was required to be three standard deviations above background. In total, AG2GUI has been able to calculate an equivalent dose and its associated error for 110 grains (44

Without any further exclusion criteria a central dose recover ratio of 1.038 ± 0.015 and an overdispersion of 13 % were found (Fig. 5). The average recuperation ratio of the entire data set was 0.06, with 100 % (90 %, 50 %) of the grains exhibiting a recuperation ratio < 0.15 (< 0.1, < 0.05). Approximately 77 % (53 %, 30 %) of the grains showed a recycling ratio between 0.8 and 1.2 (0.9 and 1.1, 0.95 and 1.05).

Applying a recuperation threshold of 0.05 did not yield significant improvement, both in dose recover ratio (CAM: 1.012 ± 0.019) and overdispersion (12.1 %). In contrast, an additional recycling ratio criterion of 0.1 reduced the overdispersion to 7.6 %.

5. Discussion and conclusion

The presented approach shows that both the attribution of OSL signal to specific grains and the aliquot movement can be successfully automatized for the needs of single grain dose determination by image processing. Although the success rate of the segmentation procedure

is already encouraging, the employment of additional image processing tools (e.g. better thresholding, flat-field correction and deblurring techniques) and/or further development of the optic system should be pursued to allow higher identification rate, even under less ideal (and less artificial) arrangements of grain on the sample disc.

While the dose recovery test could successfully determine the equivalent dose and a reasonable overdispersion, these experiments do not allow yet assessing the full performance of the system, as this study was performed on well bleached homogeneously irradiated and separated grains, so any potential signal cross talk effects are minimized and not visible in the results. The importance of investigating the impact of this phenomenon in a following study has to be stressed. Even more, as the images are still subject of heavy blurring which most likely enhanced cross talk.

Appropriate signal-to-noise levels seem at a first glance - to be most challenging when using grains with lower radiation sensitivity and/or lower doses. For imaging devices such as EM-CCDs, the signal per pixel is inevitably lower than that of an integrating device. However, noise cannot only be minimized by longer exposure time, but also lower resolution (e.g. binning per ROI). On the other hand, one is not able to minimize read-out noise beyond a certain limit with these methods. Thus, new expertise in the trade-off of time and spatial resolution has to be sought for this technique. Another solution to increase signal-to-noise ratio would be the adoption of an alternative signal acquisition and progression technique, called high pixel rate photon counting see [5, 6]. While the used camera is technically capable of applying this technique, the practicability remains to be evaluated.

Author information

S.G. and N.G. share first authorship.

Author contribution

S.G. and N.G. initiated the study and wrote the manuscript, D.M. contributed paragraphs on the lexsyg hardware and AG2GUI. N.G. carried out the measurements. S.G. developed

the AG2, D.M. the AG2GUI software and the ImageJ functionality. All authors revised and approved the manuscript.

Acknowledgements

We dedicate this article to our late friend and colleague Matthias Krbetschek. His scientific expertise and personal motivation were essential in the development of this method. Special thanks to Steve Grehl and Michael Richter (both Freiberg Instruments) which helped in Programming the AG2GUI.

References

References

[1] L.J. Arnold, M. Demuro, and M. Navazo Ruiz. Empirical insights into multi-grain averaging effects from "pseudo" single-grain OSL measurements. *Radiation Measurements 47, 652-658*, 2012.

[2] M. Ballarini, A. G. Wintle, and J. Wallinga. Spatial variation of dose rate from beta sources as measured using single grains. *Ancient TL 24, 1-8.*, 2006.

[3] J. Cardinale. Histogram-based background subtractor for ImageJ. Technical report, ETH Zurich, 2010.

[4] L. Clark-Balzan and J-L. Schwenninger. First steps toward spatially resolved osl dating with electron multiplying charged-coupled devices (EMCCDs): System design and image analysis. *Radiation Measurements 47, 797-802.*, 2012.

[5] O. Daigle, J.-L. Gach, C. Guillaume, S. Lessard, C. Carignan, and S. Blais-Ouellette. CCCP: a CCD controller for counting photons. *Proceedings of SPIE*, 7014:70146L–1, 2008. doi: 10.1117/12.788929. URL `http://dx.doi.org/10.1117/12.788929`.

[6] O. Daigle, O. Djazovski, D. Laurin, R. Doyon, and É. Artigau. Characterization results of EMCCDs for extreme low-light imaging. In *Society of Photo-Optical Instrumentation Engineers (SPIE) Conference Series*, volume 8453 of *Society of Photo-Optical Instrumentation Engineers (SPIE) Conference Series*, page 3, July 2012. doi: 10.1117/12.926385.

[7] G.A.T. Duller. Assessing the error on equivalent dose estimates derived from single aliquot regenerative dose measurements. *Anci*, 25:15–24, 2007.

[8] G.A.T. Duller, L. Bøtter-Jensen, P. Kohsiek, and A. S. Murray. A high-sensitivity optically stimulated luminescence scanning system for measurement of single sand-sized

grains. radiation protection dosimetry 84, 325-330. *Radiation Protection Dosimetry 84, 325-330.*, 1999.

[9] T. Ferreira and W. S. Rasband. *ImageJ users guide.* http://rsb.info.nih.gov/ij/docs/guide/user-guide.pdf, 1.46r edition, 2012.

[10] R.F. Galbraith and P.F. Green. Estimating the component ages in a finite mixture. *Nuclear Tracks and Radiation Measurements 17, 197-206.*, 1990.

[11] R.F. Galbraith, R.G. Roberts, G.M. Laslett, H. Yoshida, and J.M. Olley. Optical dating of single and multiple grains of quartz from jinmium rock shelter, northern australia: Part I, experimental design and statistical models. *Archaeometry 41, 339-64.*, 1999.

[12] S. Greilich and G. Wagner. Development of a spatially resolved dating technique using HR-OSL. *Radiation Measurements 41, 738-743.*, 2006.

[13] S. Greilich, U.A. Glasmacher, and G.A. Wagner. Spatially resolved detection of luminescence: a unique tool for archaeochronometry. *Naturwissenschaften 89, 371-375.*, 2002.

[14] S. Greilich, H.L. Harney, C. Woda, and G.A. Wagner. AgesGalore - a software program for evaluating spatially resolved luminescence data. *Radiation Measurements 41, 726-735.*, 2006.

[15] Princeton Instruments. ProEM+ EMCCD camera system manual. Technical report, Princeton Instruments, 2012.

[16] Princeton Instruments. Novel, performance-enhancing CCD technology - a primer on eXcelon technology. Technical report, Princeton Instruments, 2012.

[17] M. Lamothe, S. Balescu, and M. Auclair. Natural IRSL intensities and apparent luminescence ages of single feldspar grains extracted from partially bleached sediments. *Radiation Measurements 23, 555-561.*, 1994.

[18] D. Mittelstraß. *AgesGalore2GUI guideline*. Freiberg Instruments GmbH, Freiberg, 2014.

[19] A. S. Murray and R. G. Roberts. Determining the burial time of single grains of quartz using optically stimulated luminescence. *Earth and Planetary Science Letters 152, 163-180.*, 1997.

[20] A.S. Murray and A.G. Wintle. Luminescence dating of quartz using an improved single-aliquot regenerative-dose protocol. *Radiation measurements*, 32(1):57–73, 2000.

[21] J.M. Olley, G.G. Caitcheon, and R.G. Roberts. The origin of dose distributions in fluvial sediments, and the prospect of dating single grains from fluvial deposits using optically stimulated luminescence. *Radiation Measurements 30, 207?217.*, 1999.

[22] S.S. Pfeifer and M.R. Krbetschek. Radioluminescence investigations on alumosilicates for age determination. *Verhandlungen der Deutschen Physikalischen Gesellschaft. March 22-27. Dresden, Germany. Dielectric solids division overview of invited talks and sessions, 18.*, 2009.

[23] D. Richter, R. Pintaske, K. Dornich, and M. Krbetscheck. A novel beta source design for uniform irradiation in dosimetric applications. *Ancient TL*, 30:57–64, 2012.

[24] D. Richter, A. Richter, and K. Dornich. lexsyg - a new system for luminescence research. *Geochronometria*, pages 1–9, 2013.

[25] T.W. Ridler and S. Calvard. Picture thresholding using an iterative selection method. *Systems, Man and Cybernetics, IEEE Transactions on*, 8(8):630–632, Aug 1978. ISSN 0018-9472. doi: 10.1109/TSMC.1978.4310039.

[26] D. Rufer and F. Preusser. Potential of autoradiography to detect spatially resolved radiation patterns in the context of trapped charge dating. *Geochronometria 34, 1-13.*, 2009.

[27] C.A. Schneider, W.S. Rasband, and K.W. Eliceiri. NIH Image to ImageJ: 25 years of image analysis. *Nat Meth*, 9(7):671–675, July 2012. ISSN 1548-7091. URL `http://dx.doi.org/10.1038/nmeth.2089`.

[28] Roper Scientific. On-chip multiplication gain (technical note #14). Technical report, Princeton Instruments, 2002.

[29] P. Thvenaz, U.E. Ruttimann, and M. Unser. A pyramid approach to subpixel registration based on intensity. *IEEE Transactions on Image Processing, vol. 7, no. 1, pp. 27-41.*, 1998.

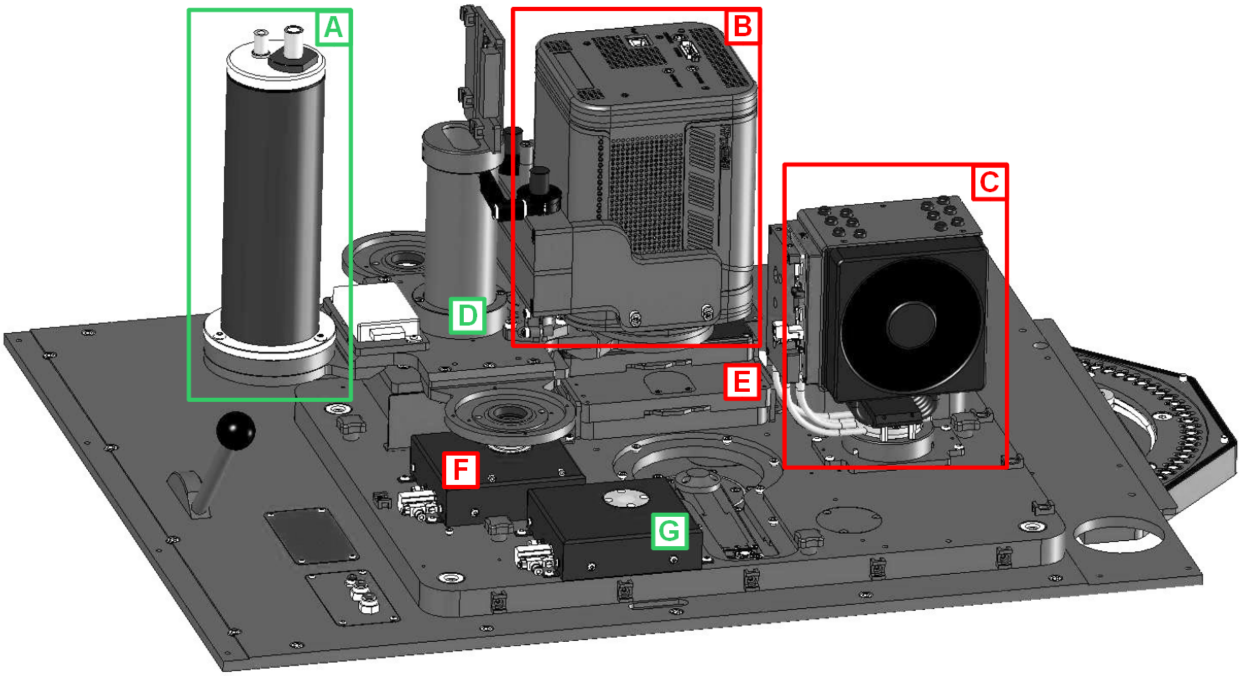

Figure 1: Schematic build-up of the Lexsyg re007 "Delorean" detection and stimulation unit. Green framed units were not used in the experiments: A: ET Enterprises 9235Q photo multiplier. B: Princeton Instruments ProEM512B eXcelon camera. C: solar simulator. D: detector changer. E: multi-wavelength OSL/IRSL-stimulation unit with two 6x filter wheels attached. F: 1.95 GBq high homogeneous ring β-source. G: 1.85 GBq high dose rate overhead β-source.

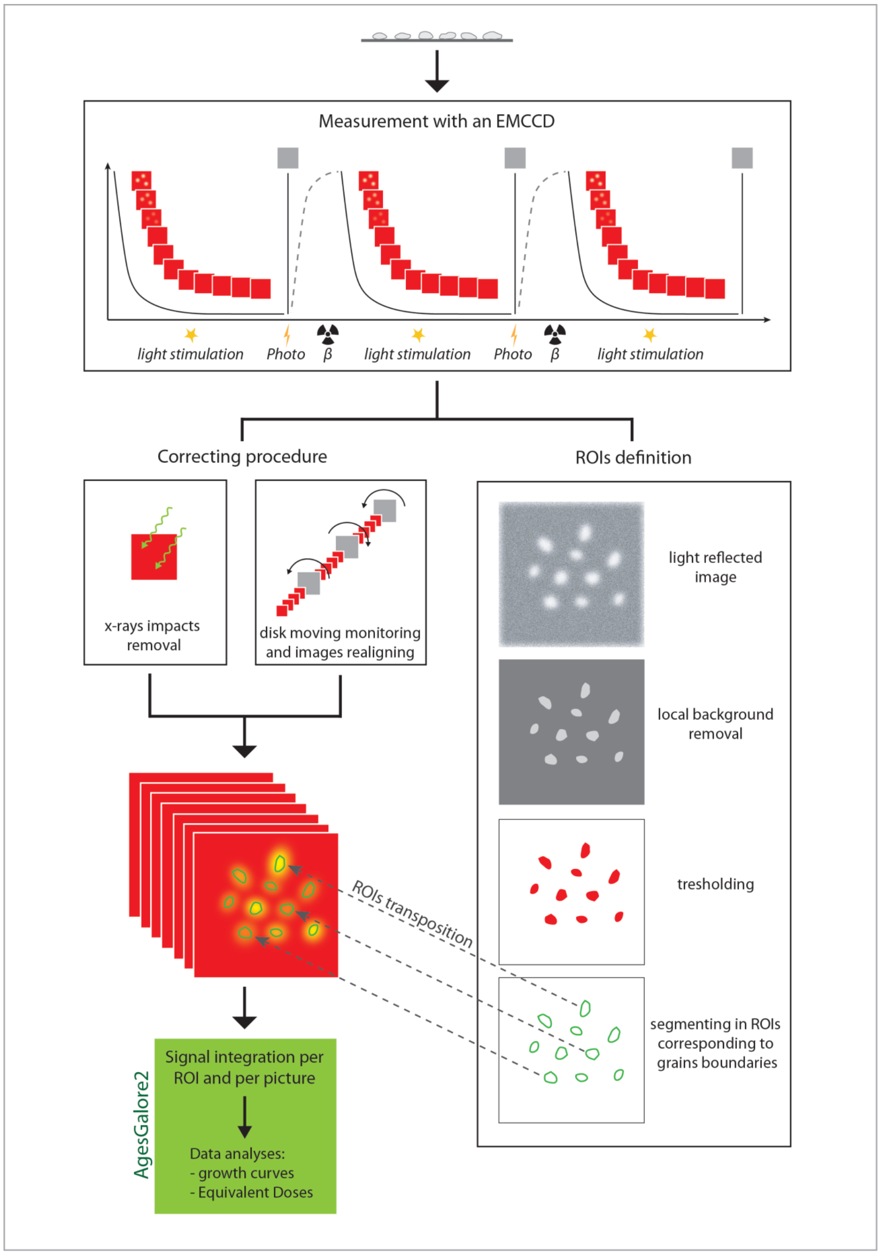

Figure 2: Workflow of single grain OSL dose recovery tests.

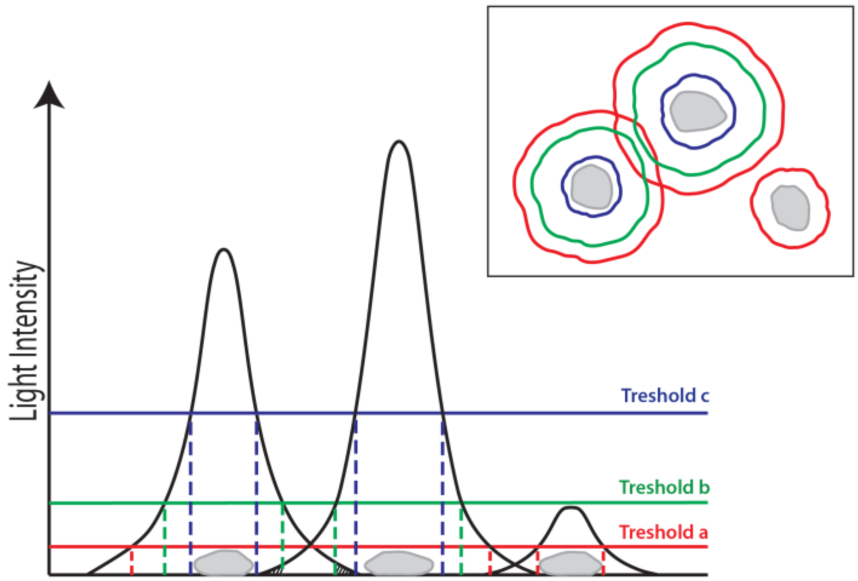

Figure 3: Illustration of thresholding luminescent images. In case, the threshold value is too low (a) the algorithm will not be able to separate the influence sphere per grain in case of two bright grains next close by. In such a situation, it is necessary to increase the value (b, c), but this will lead to disregard dimer grains.

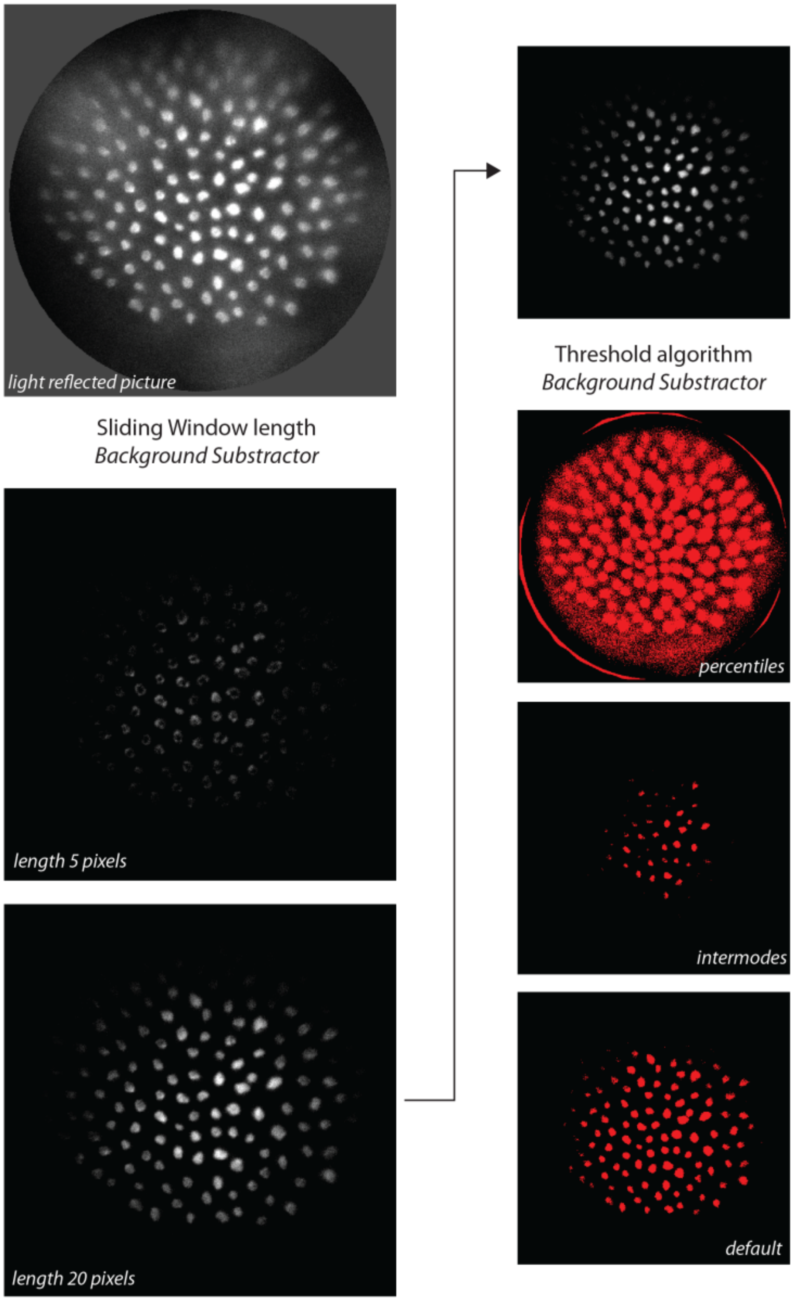

Figure 4: Impact of parameter choice on image quality and segmentation outcome. Left: example of a length too small and an appropriate value for the sliding window side length (Background Substractor). Right: resulting binary image of the percentiles, intermodes and default algorithm for thresholding.

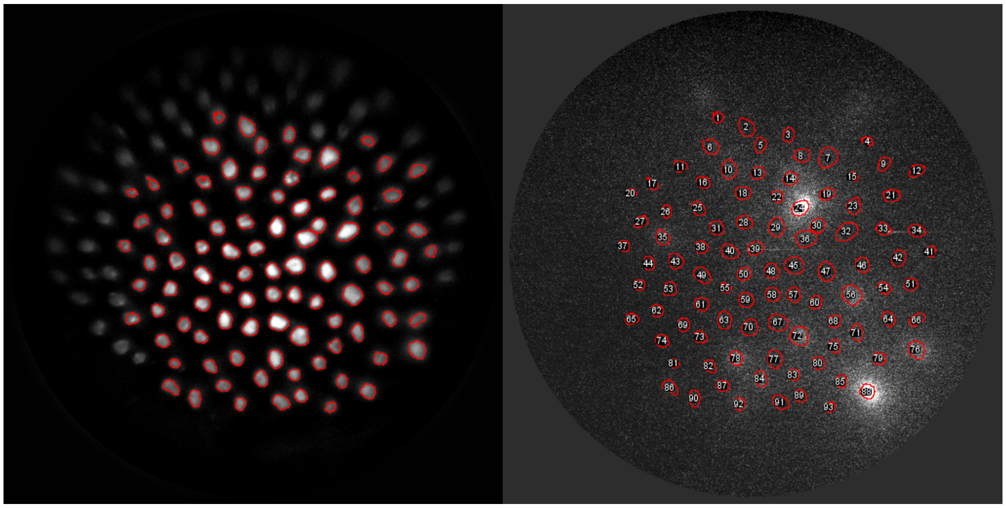

Figure 5: Example of ROI segmentation from the light reflected picture (left) and ROIs transposed over the luminescence picture recording the natural signal (right).

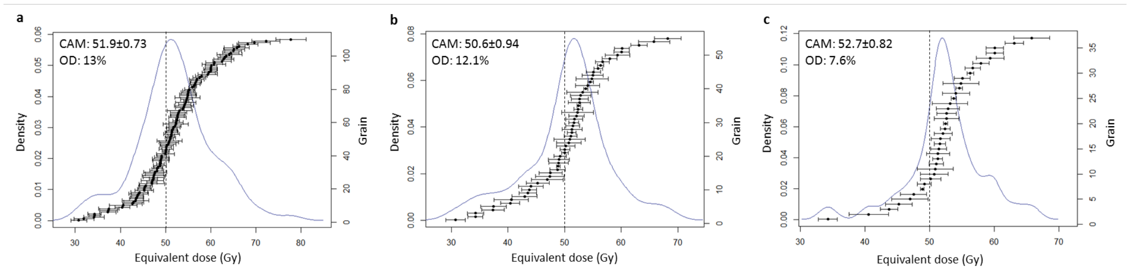

Figure 6: Single-grain equivalent-dose distribution for a) for the entire data set [UNIT DOSE: GY!!], b) with a recuperation threshold of 0.05 is applied, and c) a recuperation threshold of 0.05 and a recycling criteria between 0.9 and 1.1 applied.

Dose (artificial nat. 50 Gy; reg. 25 Gy, 50 Gy, 100 Gy, 0 Gy, 25 Gy)
Preheat 230 C for 10 s
BlueOSL stimulation 30 s at 125 C
Reflected light photo
Sunlight simulator bleaching 150 s
Test Dose (25 Gy)
Preheat 230 C for 10 s
BlueOSL stimulation 30 s at 125 C
Reflected light photo
Sunlight simulator bleaching 150 s

Table 1: DRT protocol & details

Length window BG substractor	TS algorithm	min size particle	min circularity particle	ROIs/ total number of grains	Matching ROI to grain
5	Default dark	50	0.1	68 %	Bad: several ROIs included in one grain area
20	Default dark	50	0.1	74 %	Good: ROIs defined correspond to grains
20	Intermodes dark	50	0.1	115 %	Bad: ROIs do not correspond to grains and/or are much larger that grain surfaces
20	Moments dark	50	0.1	17 %	Good: ROIs defined correspond to grains (but many are ignored)
20	Default dark	10	0.1	82 %	Mitigate: some ROIs are much smaller than grain surface
20	Default dark	100	0.1	62 %	Good: ROIs defined correspond to grains (but some ignored as too small)
20	Default dark	50	0.8	61 %	Good: ROIs defined correspond to grains (but some ignored are not round enough)

Table 2: Grain identification

A. Data processing in AgesGalore2

A real-world detector is mimicked in AgesGalore2 as a set of functions f representing its properties to infer the actual number of photons arrivals λ at the detector and the corresponding uncertainty[4] $\Delta\lambda$ from the raw digital signal $\tilde{z}$ ("intensity", "counts") that has been recorded. We follow the nomenclature used in [14]. The raw signal ("counts", "intensity") can be described as a series of data points indexed by n taken over several periods of time m:

$$\tilde{z}_{n,m} \tag{A.1}$$

In case of PMT data $n = 1$ and m describes the "channels" (time intervals). For image-based luminescence data, n runs either over the pixels of an entire image OR the pixels that have been defined as a region of interest (ROI, e.g. a single grain) – while m runs over the image frames taken subsequently as a series of time intervals, corresponding to the *channels* in the PMT case. The raw signal $\tilde{z}$ will therefore be first summed over a chosen subset of n and m, e.g. a ROI and multiple channels:

$$\tilde{z} = \sum_{m=1}^{M} \sum_{n=1}^{N} \tilde{z}_{n,m} \tag{A.2}$$

The unit of $\tilde{z}$ is assumed to be "counts" (although strickly spoken the quantity is mostly unitless).

A.1. From raw signal to net signal

The net signal is derived by ([15, 28]):

$$z = \tilde{z} - N \cdot M \cdot (\xi + z_{\text{dark}} + z_{\text{Xray}}) \tag{A.3}$$

where the notation has been adapted to this document and ξ denotes the bias (background). z_{dark} arises due to the thermal creation of additional charge (electrons) and is

[4] All uncertainties are reported as *standard uncertainty* ($1\,\sigma$)

estimated by

$$z_{\text{dark}} = n_{\text{dark}}^{e^-} \cdot \Delta t \cdot G/C \tag{A.4}$$

where $n_{\text{dark}}^{e^-}$ is the thermal charge generation rate (unit: "number of electrons per second"). For a typical EMCCD camera, $n_{\text{dark}}^{e^-}$ is approximately $10^{-3}\ e^-/s$ at $-70\,C$.

z_{Xray} is the additional signal due to impact of photons from the build-in radioactive source. Since it was effectively removed by image processing, it was neglected here.

A.2. From net signal to photon arrivals

The number of photo electrons corresponding to a net signal z can be expressed as

$$n^{e^-} = z \cdot \frac{C}{G} \tag{A.5}$$

and the photon arrivals then be derived from the number of electrons by

$$\lambda = \frac{n^{e^-}}{\eta} = \frac{z}{\eta} \cdot \frac{C}{G} \tag{A.6}$$

where η is the quantum efficiency which is here for the sake of simplicity set to unity, i.e.

$$\lambda = z \cdot \frac{C}{G} \tag{A.7}$$

Unphysical, negative photon arrival values can occur at low signals, since z can be negative (see Eq. A.3). Arithmetical operations, e.g. subtraction of two photon arrival values $\lambda_1 - \lambda_2 = \lambda_3$ with λ_3 being close to zero can strictly spoken be performed in a straight forward manner. While approaches exist to tackle this issue [14], we neglected this fact in this study for the sake of simplicity and discarded too low signals.

The uncertainty in photon arrivals is both determined by the shot noise ($\sqrt{(}\lambda)$) and the electronic read out noise σ_{readout}. σ_{readout} describes the variation (standard uncertainty) during amplification process and is given in "number of electrons". It is not influenced by G. A typical value for an EMCCD system is $2 - 3\ e^-$.

$$\Delta\lambda = \sqrt{\lambda + N \cdot M \cdot \left(\frac{\sigma_{\mathrm{readout}}}{\eta}\right)^2} = \sqrt{\lambda + N \cdot M \cdot \sigma^2_{\mathrm{readout}}} \tag{A.8}$$

To make the photon arrivals comparable if summed over time intervals of different length, the arrival rate λ is defined by

$$\Lambda = \frac{\lambda}{M \cdot \Delta t} \tag{A.9}$$

where Δt is the length of a time interval (frame, channel) in seconds.

A.3. MASS protocol

The Multiple Area Single Section (MASS) protocol is an extension of the well-known SAR protocol (*single aliquot regeneration*, [20]) to multipoint data, e.g. pixels of images, assuming that each data point represents its own independent source of light and dose/age information, respectively. Thus, MASS performs a SAR protocol on each point (yielding e.g. new images of spatial equivalent dose distribution, goodness of fit etc.) *and* on groups of points that have been binned on the level of the raw signal data, i.e. *regions of interest* (ROIs, e.g. for single grains)[5]. MASS uses the photon arrival rates from multiple ($n > 1$) regeneration measurements

$$\Lambda_{\mathrm{reg}}(D_i, m_1, m_2) \tag{A.10}$$

where D_i are the regeneration doses (with $i = 1...k$, $k > 1$ and $D_i \neq D_j$ for at least one combination of i and j) and m_1, m_2 the first and last time interval the raw signal was summed over, respectively, with $m_2 \geq m_1$. A "background signal", obtained from later

[5]This means especially that – as described in section A – the summed ROI raw signal data first are converted into photon arrivals and then used to establish a growth curve. This is an important difference between AgesGalore and AgesGalore2. AgesGalore computed equivalent doses for each pixel first and *then* binned/averaged them to a ROI equivalent dose.

channels / image frames in the shine-down curve is used for correction, so that L_X is defined as:

$$L_\mathrm{X} = \Lambda_\mathrm{reg}^\mathrm{foreground}(D_i, m_1, m_2) - \Lambda_\mathrm{reg}^\mathrm{background}(D_i, m_3, m_4) \tag{A.11}$$

with $m_4 \geq m_3 > m_2$. The corresponding test dose data $\Lambda_\mathrm{reg}^\mathrm{test}(D_i^\mathrm{test}, \tilde{z})$ are used to get T_X:

$$T_\mathrm{X} = \Lambda_\mathrm{reg}^\mathrm{test}(D_i^\mathrm{test}, m_1, m_2) - \Lambda_\mathrm{reg}^\mathrm{test}(D_i^\mathrm{test}, m_3, m_4) \tag{A.12}$$

All D_i^test have to have the same magnitude. Eventually, $\tilde{L}_\mathrm{X} = L_\mathrm{X}/T_\mathrm{X}$ constitute the points of the dose response (growth curve).

A.4. Equivalent dose

To compute the equivalent dose D_eq, AgesGalore2 performs curve-fitting to the $\tilde{L}_\mathrm{X}$ values assuming a functional dependency $f_\mathrm{fit}(D, p_i)$ on dose D and a set of m parameters p_i. We chose an exponential saturation ($m = 3$):

$$y = p_1 \cdot (1 - \mathrm{e}^{-x/p_2}) + p_3 \tag{A.13}$$

With the best set of parameters $\hat{p}_i$ found, the natural signal $\tilde{L}_\mathrm{nat}$ is computed in the same way as $\tilde{L}_\mathrm{X}$. D_eq is estimated using the model equation based on the reverse of f_fit and the best set of parameters:

$$D_\mathrm{eq} = f_\mathrm{fit}^{-1}(\tilde{L}_\mathrm{nat}, \hat{p}_i) \tag{A.14}$$

To estimate ΔD_eq, AgesGalore2 resamples the growth curve elements $\tilde{L}_\mathrm{X}$ and $\tilde{L}_\mathrm{nat}$ according to their corresponding uncertainty and assuming a normal distribution (i.e. parametric bootstrapping). This process is repeated 100 times and the standard deviation of the 100 individual D_eq results is reported as ΔD_eq.

A.5. Test criteria

AgesGalore2computes a number of test criteria partly as given by [20] and partly specific to the characteristics of pixelized data to check the integrity of the growth curve. This can be done both on a ROI and on the pixel level. The recycling ratio R is computed by dividing $\tilde{L}_1$ for the lowest (first) regenerated dose $D_1 > 0$) by the recycled signal $\tilde{L}_{\mathrm{rec}}$

$$R = \frac{\tilde{L}_1(D_1)}{\tilde{L}_{\mathrm{rec}}(D_1)} \tag{A.15}$$

The $\tilde{L}_{\mathrm{rec}}$ is recorded after the regenerated signals and has to have the same dose D_1. AgesGalore22 can – although not intended by [20] computer multiple recycling ratios if more than one recycled dose exists. The recuperation rate r is defined as the ratio of the last regenerated signal that followed an irradiation with dose 0, $\tilde{L}_{\mathrm{X}}(0)$, and the natural signal $\tilde{L}_{\mathrm{nat}}$:

$$r = \frac{\tilde{L}_{\mathrm{X}}(0)}{\tilde{L}_{\mathrm{nat}}} \tag{A.16}$$

As a measure of the discrimination between signal and background, AgesGalore2 computes a SNR according to:

$$S = \frac{\tilde{L}_{\mathrm{nat}}}{\Delta\tilde{L}_{\mathrm{nat}}} \tag{A.17}$$